Energy & Environmental Science

ROYAL SOCIETY OF CHEMISTRY

PAPER

View Article Online
View Journal | View Issue

Cite this: *Energy Environ. Sci.*, 2021, **14**, 5377

The impact of binary water–CO_2 isotherm models on the optimal performance of sorbent-based direct air capture processes†

John Young, * Enrique García-Díez, Susana Garcia and Mijndert van der Spek *

Direct air capture (DAC) is an auspicious technology in pursuing negative CO_2 emissions. A promising process is temperature vacuum swing adsorption (TVSA) employing amine functionalised adsorbents such as Lewatit® VP OC 1065, which is selected as a benchmark sorbent in this study. To further improve process design, and critically lower costs, detailed modelling of DAC cycles is imperative. However, the multi-component adsorption on these materials, particularly the cooperative adsorption of CO_2 and H_2O, is crudely understood, and yet to be described in mathematical terms, prohibiting sound modelling efforts. Here, we commit in-depth understanding of the effect of humidity on CO_2 adsorption and demonstrate how this impacts modelling of DAC cycles. We present two novel mechanistic co-adsorption isotherm models to describe water's effect on CO_2 adsorption and find a good fit to original experimental co-adsorption data. We also show the considerable improvement in predictions of these models when compared to an empirical co-adsorption isotherm model from literature. A detailed TVSA DAC cycle process model is then used elucidating how different co-adsorption models affect the predicted process performance. It is found that the two novel isotherm models generate similar results and Pareto fronts, whilst the minimum work equivalent calculated using the more conservative of the two models is found to be 2.49 MJ kg^{-1} for the case study considered. These mathematical descriptions laid out will lead to more accurate modelling and optimisation of cyclic DAC adsorption processes, prompting a greater understanding of the material-process combinations ideal for DAC and how costs can be driven down in the years to come. Importantly, they allowed us to independently benchmark a Climeworks type DAC process, providing key DAC performance data to the public domain.

Received 27th April 2021,
Accepted 2nd August 2021

DOI: 10.1039/d1ee01272j

rsc.li/ees

Broader context

Carbon dioxide removal (CDR) technologies are at the centre of scientific and public debate and policymaking. They encompass a suite of processes and systems that actively remove CO_2 from the atmosphere, aiming to store the CO_2 permanently or to utilise it, for instance, to create jet fuels. Examples of CDR are bioenergy with CO_2 capture and storage (BECCS), enhanced weathering and ocean alkalinity, land-based methods, and direct air capture (DAC), discussed here. The key questions for all these systems include: 'how much CO_2 can they remove at what land footprint?'; 'how much does this cost in terms of energy, physical inputs/outputs and money?'; and 'how much can we bring the costs down by innovation?'. These numbers are becoming well established and corroborated by independent science for some technologies, *e.g.*, BECCS. For others, this is not yet the case. For solid-sorbent DAC, we still lack detailed and reliable modelling of process performance, which can then be used to identify the window of opportunity for process improvements and cost reductions. We here provide a rigorous, detailed modelling study on adsorbent-based DAC technical performance, where newly developed water–CO_2 co-adsorption isotherm models, using a comprehensive set of experimental data, are incorporated.

1. Introduction

Anthropogenic greenhouse gas (GHG) emissions are causing the dramatically rising temperature of our planet. The level of atmospheric CO_2 and other GHGs has become untenable, and drastic action is required to prevent a global temperature rise of 1.5 °C, which has been identified as an important limit by the Intergovernmental Panel on Climate Change (IPCC).[1] Negative emissions technologies (NETs) that actively remove CO_2 from the atmosphere will be needed to mitigate hard-to-abate and historical emissions and to reach the Paris Agreement targets.[2,3] Carbon capture and storage (CCS) has a significant

Research Centre for Carbon Solutions, Heriot-Watt University, Edinburgh, EH14 4AS, UK. E-mail: jpy1@hw.ac.uk, m.van_der_spek@hw.ac.uk

† Electronic supplementary information (ESI) available. See DOI: 10.1039/d1ee01272j

role to play in the development and deployment of NETs. Two promising NETs rely on CCS technology. These are bioenergy with carbon capture and storage (BECCS) and direct air capture (DAC).[4] DAC aims to capture CO_2 directly from ambient air resulting in net negative emissions if the CO_2 is permanently stored.[5] Realmonte *et al.* explored the role DAC can play in a 1.5 °C scenario and emphasise the economic benefit that DAC provides.[5] The study finds that policymakers require much lower carbon prices when DAC is available as a technology. However, the authors of this study stress that DAC should be developed alongside other solutions since significant technical challenges exist.

1.1 Challenges in sorbent-based DAC process design

Here, we focus on direct air capture of CO_2 using amine functionalised adsorbents in temperature vacuum swing adsorption (TVSA) processes. Thus far, much research effort in this space has gone to the development of effective, robust and cheap sorbent materials. More information is available in the ESI,† as well as Table S1 which summarises some of the materials studied for DAC to date. Beyond sorbent development, the main current challenge for adsorbent-based DAC technologies is to further optimise their process design to enhance efficiency and reduce cost. For this, two critical elements are needed: (i) detailed cyclic adsorption process modelling to find optimal process cycles and operating parameters, requiring (ii) accurate mathematical descriptions of the underlying adsorption of each adsorbed component, with a focus on the interaction between CO_2 and H_2O. Without accurate adsorption descriptions, there is simply little point in undertaking process design studies.

The two facets governing adsorption that need to be mathematically described are adsorption equilibrium and dynamics (*i.e.*, mass transfer), and this is done using isotherm and kinetic models, respectively. Casas *et al.* explain that adsorption process modelling is susceptible to small errors in isotherm models, emphasising the importance of an accurate description, and developing the required isotherm models will be one of the objectives of this work.[6] As humidity in air is reported to enhance the equilibrium adsorption of CO_2 on amine-functionalised adsorbents, it is pivotal to describe this interaction correctly.[7–10] However, a mechanistically consistent mathematical description of this enhancement does not yet exist, impeding accurate modelling of DAC processes, and therefore their further improvement.

Here, we aim to fill the caveats in understanding and modelling of water–CO_2 interactions, by deriving mechanistically consistent co-adsorption models, showing how the use of different models influences the modelling of DAC adsorption cycles and thus their technical performance. To this end, we combined adsorption theory with new experiments and modelling studies. The paper is structured as follows: first, the theoretical mechanisms and their implications for CO_2 adsorption onto amine-functionalised sorbents are discussed to allow the derivation of sound (co-)adsorption isotherm models. Second, accurate representations of pure component and co-adsorption isotherms were measured experimentally and fit to the co-adsorption isotherm models. Finally, the isotherm models were used in a detailed process model to demonstrate how the different descriptions affect process performance and assert that sound descriptions of the physical processes are indeed critical to the design of efficient sorbent-based DAC plants.

In this work we use Lewatit® VP OC 1065 as an example of a typical primary amine-functionalised adsorbent and we suggest henceforth to use this sorbent as a *benchmark* for DAC purposes. A key reason to select this sorbent is its commercial availability, and therefore accessibility to any interested party, besides being believed to be (very similar to) the adsorbent that Climeworks uses in their first-generation DAC process.‡

2. Theory of CO_2 and H_2O adsorption onto amine-functionalised adsorbents

2.1 Pure component adsorption

2.1.1 CO_2 isotherms. Adsorption equilibrium of species onto a solid surface is typically described by isotherm models. A standard isotherm model used to describe CO_2 adsorption on amine-functionalised adsorbents is the temperature-dependent Toth isotherm which has previously been used for amine functionalised silica, cellulose, and Lewatit® VP OC 1065.[7,11–13] This is an empirical extension to the Langmuir isotherm, which improves the fit at the lowest and highest pressure ranges,[14] the lowest region being specifically relevant for amine functionalised sorbents due to their high affinity for CO_2. The equations defining the temperature-dependent form of the Toth isotherm are given in eqn (1)–(4).

$$q_{CO_2} = \frac{q_\infty(T) b(T) p_{CO_2}}{\left(1 + \left(b(T) p_{CO_2}\right)^{\tau(T)}\right)^{\frac{1}{\tau(T)}}} \quad (1)$$

where q_{CO_2} [mol kg^{-1}] is the loading of CO_2 on the adsorbent, q_∞ [mol kg^{-1}] is maximum CO_2 capacity, b [Pa^{-1}] is the affinity of CO_2 to the adsorbent, p_{CO_2} [Pa] is the partial pressure of CO_2, and τ [—] is an exponential factor to account for surface heterogeneity. The maximum CO_2 capacity of the sorbent is defined by eqn (2).

$$q_\infty(T) = q_{\infty,0} \exp\left(\chi\left(1 - \frac{T}{T_0}\right)\right) \quad (2)$$

where $q_{\infty,0}$ [mol kg^{-1}] is q_∞ at the reference temperature T_0 [K], T [K] is the temperature, and χ [—] is a factor used to describe the temperature dependency.

The affinity of the sorbent to CO_2 is defined by eqn (3).§

$$b(T) = b_0 \exp\left(\frac{-\Delta H_0}{RT}\right) \quad (3)$$

‡ Climeworks' patent describing the kind of material that may be used in their process and simultaneously supplying an accurate description of Lewatit® VP OC 1065: "polystyrene matrix material modified with amine groups, specifically primary amine groups".[57]

§ The equation more commonly used to describe this parameter[13] has been rearranged in this work, which also changes the meaning of b_0. The original equation causes the relationship between ΔH_0 and b to be dependent on the arbitrarily assigned T_0. For this reason, the equation has been changed to remove this dependence, and the motivation becomes apparent in Section 2.3.1, where ΔH_0 is a parameter that varies due to co-adsorption.

where b_0 [Pa^{-1}] is a pre-exponential affinity parameter, ΔH_0 [J mol^{-1}] is the isosteric heat of adsorption, and R [J mol^{-1} K^{-1}] is the universal gas constant. Finally, the surface heterogeneity parameter is defined in eqn (4).

$$\tau(T) = \tau_0 + \alpha\left(1 - \frac{T_0}{T}\right) \quad (4)$$

where τ_0 [—] is τ at the reference temperature, and α [—] is a factor used to describe the temperature dependency.

2.1.2 H_2O isotherms. Adsorption of water onto solid species is an interesting field of study itself and is essential for CO_2 capture applications. The work by Hefti *et al.*,[15–18] provides a very relevant body of knowledge. Water adsorption on Lewatit® VP OC 1065 follows a typical Type III isotherm, with hysteresis loops of Type H3, according to the IUPAC classification.[19] The isotherms can be seen in Fig. S10, in the ESI.† This behaviour is typical for unrestricted monolayer-multilayer adsorption of the water onto favourable sites of a macroporous adsorbent.

We chose an isotherm model that is commonly used to describe this behaviour, *i.e.*, the Guggenheim–Anderson–de Boer (GAB) model.[7,13,20] This model is an extension to the widely utilised Brunauer–Emmett–Teller (BET) equation.[61] The derivation of the BET equation assumes that the first layer of adsorption has a heat of adsorption that is different from every subsequent layer, whilst the subsequent layers have a heat of adsorption equivalent to the latent heat of condensation. Meanwhile, the GAB model improves this by assuming that only the 10th layer onwards has a heat of adsorption equal to the latent heat of condensation, whilst the 2nd to 9th layers have a heat of adsorption that is different to the first layer. eqn (5) presents the GAB isotherm model:

$$q_{H_2O} = \frac{q_m kcx}{(1 - kx)(1 + (c - 1)kx)} \quad (5)$$

where q_{H_2O} [mol kg^{-1}] is the loading of water, q_m [mol kg^{-1}] is the loading that corresponds to a monolayer, k [—], and c [—] are affinity parameters, and x [—] is the relative humidity.

Some studies do not consider temperature dependency beyond its effect on relative humidity with k and c as constant values.[13,15] Other studies describe the temperature dependency of k and c according to Anderson's derivation.[7,16,20,21] These descriptions as they appear in Anderson's derivation are shown in eqn (6) and (7).[21,22] Note that the pre-exponential factors used in the recent studies by Gebald *et al.*[7] and Wurzbacher *et al.*[20] are dropped to present the description according to Anderson's derivation.

$$c = \exp\left(\frac{E_1 - E_{10+}}{RT}\right) \quad (6)$$

where E_1 [J mol^{-1}] is the heat of adsorption of the first layer of adsorption, and E_{10+} [J mol^{-1}] is the heat of adsorption of the 10th layer and higher, which is equivalent to the latent heat of condensation of water.

$$k = \exp\left(\frac{E_{2-9} - E_{10+}}{RT}\right) \quad (7)$$

where E_{2-9} [J mol^{-1}] is the heat of adsorption of the 2nd to 9th layer.

The picture is further complicated when it is considered that the heats of adsorption of the different layers may also be dependent on temperature, as is found by Anderson and Hall.[22] Indeed, we know that the heat of condensation for water, or E_{10+}, depends on temperature.

Here, we chose to incorporate the temperature dependency because our experimental results show a temperature-dependency beyond that taken into account by relative humidity, see Fig. S10 in the ESI,† as was also found earlier by Gebald *et al.* for amine-functionalised cellulose.[7] Up to 100 °C, the thermal stability limit of Lewatit® VP OC 1065,[23] we fitted the heat of condensation for water to the correlation shown by eqn (8) using experimental data from NIST.[24]

$$E_{10+} = -44.38T + 57\,220 \quad (8)$$

Consequently, to fit an accurate version of the GAB equation, the unknown dependencies of temperature on E_1 and E_{2-9} were empirically fitted to the experimental water isotherms measured in this study.

2.2 Effect of humidity on CO_2 adsorption

On amine-functionalised adsorbents, it has been shown that CO_2 has little impact on H_2O equilibrium adsorption up to relative humidities of at least 60%.[7,8,25] However, previous studies have shown that H_2O enhances CO_2 adsorption significantly.[7–9,26,27]

The underlying chemical mechanisms need to be understood in detail to mathematically explain the co-adsorption of CO_2 and H_2O on amine-functionalised sorbents. Thus far, there has been only one attempt to develop an empirical mathematical description by Stampi-Bombelli *et al.*,[13] further discussed in Section 2.3.3. Meanwhile, Jung and Lee derived an isotherm model from kinetics specifically for ammonium carbamate and bicarbonate formation.[28] However, there is no one adsorption mechanism that is valid for all amine-functionalised sorbents, and actually, there may be multiple mechanisms in play on one adsorbent.

Here, we briefly discuss the key mechanisms used to derive mechanistically consistent co-adsorption isotherm models. The mechanisms are threefold: the change of amine efficiency (*i.e.*, CO_2 adsorption stoichiometry); a change in the heat of adsorption, also affecting the sorbent's affinity to CO_2; and amine site blocking by adsorbed water molecules.

2.2.1 Three governing mechanisms. Existing literature has repeatedly reported the two species formed on amine functionalised adsorbents in the presence of carbon dioxide, and these are shown in Fig. 1.

Fig. 1(a) shows an ammonium carbamate ionic pair, which forms from an ammonium carbamate zwitterion precursor requiring two amine groups per adsorbed CO_2 molecule.[25,27,29–32] Meanwhile, Fig. 1(b) is a pair of carbamic acid species stabilising each other *via* hydrogen bonding.[25,27,31,33,34] The carbamic acid requires stabilisation as it tends to convert back to CO_2 and an

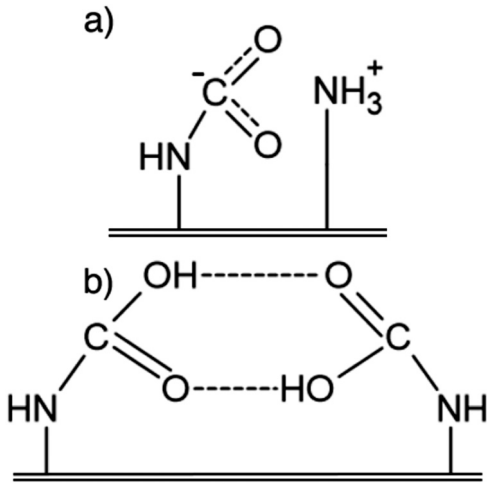

Fig. 1 Species that CO_2 adsorbs as on amine-functionalised sorbents in the absence of water. (a) Ammonium carbamate. (b) Paired carbamic acid.

amine group.[35] Yu and Chuang indicated that carbamic acid formation was primarily associated with secondary amines, using *in situ* FT-IR spectroscopy. However, there is not enough evidence to rule out carbamic acid forming on primary amines.[27] Indeed, the molecular modelling study by Buijs and De Flart in 2017 concluded that for the primary-amine based Lewatit® VP OC 1065, the formation of ammonium carbamate is unlikely, with the carbamic acid formation being a more favourable pathway. Although Alesi and Kitchin found, experimentally, that it was inconclusive as to whether carbamic acid or ammonium carbamate formation is the dominant mechanism on Lewatit® VP OC 1065.[36,37] In reality, it may be that many different species form on one amine-functionalised sorbent, which is shown to be possible by Yu and Chuang.[27]

Fig. 2 presents the additional adsorbed species of CO_2 that form in the presence of water. Fig. 2(a) shows ammonium bicarbonate, which forms from a paired ammonium carbamate precursor.[25,27] Li *et al.* suggest that, instead of ammonium bicarbonate formation, hydronium carbamate could also be formed from ammonium carbamate.[38] The effect on adsorption is very similar for both these pathways, as each species only requires one amine group for CO_2 adsorption, as opposed to two for ammonium carbamate. Finally, Fig. 2(b) shows a carbamic acid that is stabilised by a water molecule rather than another carbamic acid.[27]

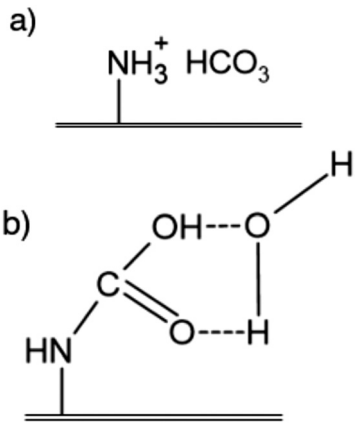

Fig. 2 Additional species that CO_2 adsorbs as on amine-functionalised sorbents in the presence of water. (a) Ammonium bicarbonate. (b) Water stabilised carbamic acid.

Kinetics may also play a role in the speciation of adsorbed carbon dioxide on amine-functionalised adsorbents. Didas *et al.* observed that the formation of ammonium bicarbonate is much slower than the formation of ammonium carbamate.[25] However, to the best of our knowledge, this has yet to be confirmed for hydronium carbamate. If ammonium bicarbonate does form more slowly from an ammonium carbamate precursor, we would expect an initially fast uptake of CO_2 until the amount of ammonium carbamate reaches equilibrium, before the uptake slowly increases further as the ammonium carbamate is converted to ammonium bicarbonate. Aside from chemical kinetics, the presence of water may also inhibit or enhance the diffusion of CO_2 to the amine sites affecting the overall kinetics of the adsorption process. This requires further investigation but is beyond the scope of this study.

For independent water adsorption, water molecules hydrogen bond onto the amine groups as the first adsorption layer with multiple layers forming on top also *via* hydrogen bonding as shown in Fig. 3.[27]

The above-explained chemistry determines a key concept in CO_2 adsorption onto amine sorbents, namely amine efficiency. Amine efficiency has previously been defined as the number of CO_2 molecules adsorbed divided by the total number of amine groups available.[25,30,39–42] For the formation of ammonium carbamate pairs, the theoretical maximum amine efficiency is 0.5 since this is the stoichiometric ratio of CO_2 adsorbed to amine groups required. However, when ammonium bicarbonate or hydronium carbamate forms, the theoretical maximum amine efficiency or stoichiometric ratio increases to 1. For this reason, the amine efficiency can be enhanced in the presence of water.

Besides amine efficiency, humidity has also shown to affect the heat of adsorption of adsorbed species. Yu and Chuang utilised temperature-programmed desorption to calculate each species' binding energy, which is equivalent to the heat of

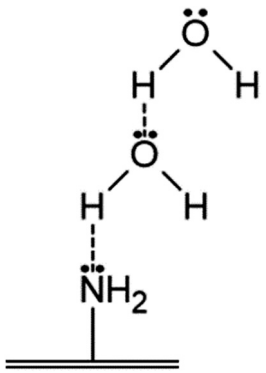

Fig. 3 Hydrogen bonding of water onto supported amine groups.

desorption. The calculations find that the binding energy increases in this order: water stabilised carbamic acid < adsorbed water < paired carbamic acid ≈ ammonium carbamate pair.[27] Their results show an apparent decrease in the overall heat of desorption in the presence of water occurring through a reduction in the binding energy of ammonium carbamate, and a promotion in the formation of ammonium bicarbonate. However, they also suggest that the presence of water increases the binding of paired carbamic acid and promotes its formation over other species leading to an overall increase in the heat of adsorption.

The heat of adsorption is not only relevant as a standalone quantity, but it also influences the uptake equilibrium, particularly the affinity constant of isotherms (see Section 2.1.1). For example, in the modified temperature-dependent version of the Toth model, shown in eqn (1)–(4), an increase in the magnitude of the heat of adsorption leads a larger affinity constant of the isotherms and *vice versa*.[12] The affinity constant is a measure of the gradient of the isotherm at low partial pressures. As a result, an increase in the heat of adsorption would lead to higher uptakes under DAC conditions because of the very low CO_2 concentrations in air.

Finally, we hypothesise there may be a third effect at play. This is water multilayers blocking CO_2 access to amine sites, which could affect kinetics and equilibrium uptake alike. Didas *et al.* observed that water can have a negative impact on CO_2 uptake at low partial pressures of CO_2 for the amine-functionalised silica they studied with the highest amine coverage.[25] We propose that the high amine coverage led to the agglomeration of water multilayers, formed on the amines, preventing CO_2 from accessing the amine sites.

2.3 Water–CO_2 co-adsorption models

The complexities in determining the exact species formed on adsorption, prevent us from using the classical kinetic approach to deriving an isotherm model. Hence, based on the above discussion, we propose two different models to consistently describe water–CO_2 co-adsorption, which we call the mechanistic co-adsorption model and the weighted average dual site Toth (WADST) model. We also discuss a recently published empirical co-adsorption model by Stampi-Bombelli *et al.*[13] Here onwards, we assume that water affects CO_2 adsorption, but CO_2 does not affect water adsorption. There is previous experimental evidence to support this assumption.[7,8,43]

2.3.1 Mechanistic co-adsorption model. To summarise, the main three effects discussed so far are:

(1) At high water loadings, amine efficiency may be limited by hydrogen-bonded water structures blocking CO_2 access to amine sites.

(2) The presence of water can increase the stoichiometric ratio due to ammonium bicarbonate forming rather than ammonium carbamate.

(3) The presence of water changes the heats of adsorption of adsorbed CO_2 species hence the affinity.

Based on these three effects, we propose the mechanistic adjustment of isotherm behaviour described in eqn (9)–(13). First, we postulate a generic equation of CO_2 loading including terms for the amine efficiency under actual, ϕ [−], and dry, ϕ_{dry} [−] conditions:

$$q_{CO_2} = \frac{\phi}{\phi_{dry}} f\left(p_{CO_2}, T, \Delta H_{ave}\right) \quad (9)$$

where f is the temperature and partial pressure-dependent isotherm equation, and ΔH_{ave} [J mol^{-1}] is the average heat of adsorption calculated in eqn (13).

Secondly, effect 1 can be described as the fraction of the sites blocked by hydrogen-bonded water structures deducted from the theoretical maximum available sites, *i.e.*, under zero site blockage, to calculate the fraction of amine sites available for adsorption as in eqn (10).

$$\phi_{available} = \phi_{max} - f_{blocked} \quad (10)$$

where $\phi_{available}$ [—] is the fraction of sites available for adsorption, and ϕ_{max} [—] is the maximum possible amine efficiency, which can be assumed to be 1 (recall this is the maximum theoretical efficiency). The fraction of the sites blocked, $f_{blocked}$ [—] must now be calculated.

Thirdly, the fraction of amine sites blocked should be proportional to the size of adsorbed water aggregates. The size of these aggregates adsorbed is further related to the loading of water on the adsorbent. We hypothesise that a parallel can be drawn between these aggregates' growth with increased loading and how crystals grow with time. Crystals nucleate and grow slowly at first. Then when the particles are of sufficient size, they begin to aggregate, speeding up the growth. At small loadings, increasing loading may only slightly increase these structures' size before reaching the critical size needed to start forming aggregates. We propose to use Avrami's equation for this purpose, as shown in eqn (11).[44–48]

$$f_{blocked} = f_{blocked,max}\left(1 - e^{-\left(kq_{H_2O}\right)^n}\right) \quad (11)$$

where $f_{blocked,max}$ [−], k [kg mol^{-1}], and n [−] are parameters to be fitted.

Next, is to describe the increase in the stoichiometric ratio and amine efficiency. As the loading of water increases, the fraction of the sites that exist with a convenient water molecule for stabilised carbamic acid or ammonium bicarbonate formation increases. We suggest that a Maxwell–Boltzmann distribution could describe this.[49,50] This distribution is used for many things relating to the probability of two states, including economics.[51] Another example is chemical kinetics, where it is used to show how, with an increase in temperature, a higher proportion of molecular collisions have the required energy for a reaction to occur (the well-known Arrhenius' law). Henceforth, we suggest applying the Maxwell–Boltzmann distribution

to our case providing eqn (12).

$$\phi = \phi_{\text{dry}} + \left(\phi_{\text{available}} - \phi_{\text{dry}}\right) e^{-\frac{A}{q_{H_2O}}} \quad (12)$$

Here A [mol kg^{-1}] is a critical water loading value that must be fitted as well as ϕ_{dry} [−].

Finally, the heat of adsorption can be calculated by taking a weighted average between the wet and dry states. Since $e^{-\frac{A}{q_{H_2O}}}$ is equal to the fraction of sites that form adsorbed species with water, the weighted average appears as in eqn (13).

$$\Delta H_{\text{ave}} = \left(1 - e^{-\frac{A}{q_{H_2O}}}\right)\Delta H_{\text{dry}} + e^{-\frac{A}{q_{H_2O}}}\Delta H_{\text{wet}} \quad (13)$$

where ΔH_{dry} [J mol^{-1}] and ΔH_{wet} [J mol^{-1}] are the heats of adsorption in dry and wet states, respectively. ΔH_{dry} can be calculated from pure CO_2 isotherms whilst ΔH_{wet} can be fit to co-adsorption data.

2.3.2 Weighted-average dual-site Toth (WADST) co-adsorption model. The derivation of the mechanistic model assumes we know everything about chemisorption of CO_2 and H_2O on amine-functionalised adsorbents, as we stated earlier, this may not yet be the case. Therefore, we propose another approach to modelling CO_2 and H_2O co-adsorption equilibrium that does not depend on these assumptions to create a more general, empirical model. To do this, we shall take a more classical approach to describe co-adsorption. This approach assumes that there are two types of site. One with an available water molecule and one without an available water molecule. Furthermore, the same approach as with the mechanistic model will be used to describe the probability that a site has an available water molecule *via* an Arrhenius style equation described by the same critical water loading parameter A. This rationale results in eqn (14).

$$q_{CO_2} = \left(1 - e^{-\frac{A}{q_{H_2O}}}\right)\frac{q_{\infty,\text{dry}}(T)b_{\text{dry}}(T)p_{CO_2}}{\left(1 + \left(b_{\text{dry}}(T)p_{CO_2}\right)^{\tau_{\text{dry}}(T)}\right)^{\frac{1}{\tau_{\text{dry}}(T)}}} + e^{-\frac{A}{q_{H_2O}}}\frac{q_{\infty,\text{wet}}(T)b_{\text{wet}}(T)p_{CO_2}}{\left(1 + \left(b_{\text{wet}}(T)p_{CO_2}\right)^{\tau_{\text{wet}}(T)}\right)^{\frac{1}{\tau_{\text{wet}}(T)}}} \quad (14)$$

Here the dry site in the isotherm is simply defined by the Toth model shown in eqn (1)–(4). Meanwhile, the wet site is again defined by the same equations and fit, alongside A, to co-adsorption experiments, with the dry site already fixed from pure-component isotherms.

2.3.3 Previous empirical co-adsorption model. Stampi-Bombelli *et al.* presented a useful first endeavour to describe co-adsorption on an amine-functionalised cellulose material by suggesting an empirical adjustment to the pure Toth model.[13] A summary of the adjustment is shown in eqn (15) and (16).

$$q_{\infty}(T, q_{H_2O}) = q_{\infty}(T)\left(\frac{1}{1 - \gamma q_{H_2O}}\right) \quad (15)$$

$$b(T, q_{H_2O}) = b(T)(1 + \beta q_{H_2O}) \quad (16)$$

Here γ [—] and β [—] do not have any specific physical meaning but are simply the parameters that describe co-adsorption and should be fit to wet experiments. The authors of this study also suggest that γ and β should be greater than 0. However, we suggest that γ could have a negative value to take into account the overall CO_2 capacity reducing due site blockage. This model is virtually the only co-adsorption model that has been investigated before and we include it in our investigations as a comparison for our models in terms of accuracy of describing the co-adsorption phenomenon and cyclic process performance.

3. Experimental methods

After formulating the mathematical adsorption equilibrium models, these needed to be parametrised with experimental data, which acquisition is described here.

The material investigated, Lewatit® VP OC 1065, was obtained from Sigma-Aldrich. It is a divinylbenzene (DVB) crosslinked polymer functionalised with primary amine groups. It has an average pore diameter of 25 nm, a bead size of 0.315–1.25 mm, pore volume of 0.27 cm^3 g^{-1}, and a surface area of 50 m^2 g^{-1}.[23] Meanwhile, the heat capacity is reported as 1.58 kJ kg^{-1} K^{-1}.[52]

CO_2 and H_2O pure component isotherms and co-adsorption isotherms were measured using the DVS Vacuum system, of which a simple schematic is depicted in Fig. 4.[54] The DVS uses a gravimetric, magnetic suspension balance to accurately measure any weight changes as a result of adsorption and desorption. It can operate in dynamic mode with gas flowing through the sorption chamber or static mode where gas is pulsed into the chamber. The DVS utilises a turbomolecular pump which ensures extremely thorough outgassing.

The methodology for measuring pure component isotherms first involved an outgassing step where around 50 mg of sample was heated to 100 °C at a pressure of around 1–2 Pa for at least 10 hours. The sample was then cooled to the desired adsorption temperature before the gas and/or vapour was fed to the device by opening the mass flow controllers. The pressure was increased stepwise up to 1 bar allowing the mass of the sample to equilibrate at each step. CO_2 sorption was studied under semi-static mode, whilst the dynamic mode was used for H_2O sorption. Once 1 bar was reached, the procedure was repeated backwards, *i.e.*, in desorption mode, providing potential hysteresis measurements. A fresh sample of adsorbent was used for every isotherm.

CO_2–water co-adsorption isotherm experiments were undertaken using the DVS Vacuum under the explicit assumption that CO_2 does not affect H_2O equilibrium adsorption. This was demonstrated by Veneman *et al.* for Lewatit up to a relative humidity of 60%.[8] In addition, there is evidence that this assumption also holds for other types of amine-functionalised adsorbents, such as silica and cellulose.[7,25] For the co-adsorption experiments, the outgassing step was the same, and semi-static mode was used. Then, the sample was

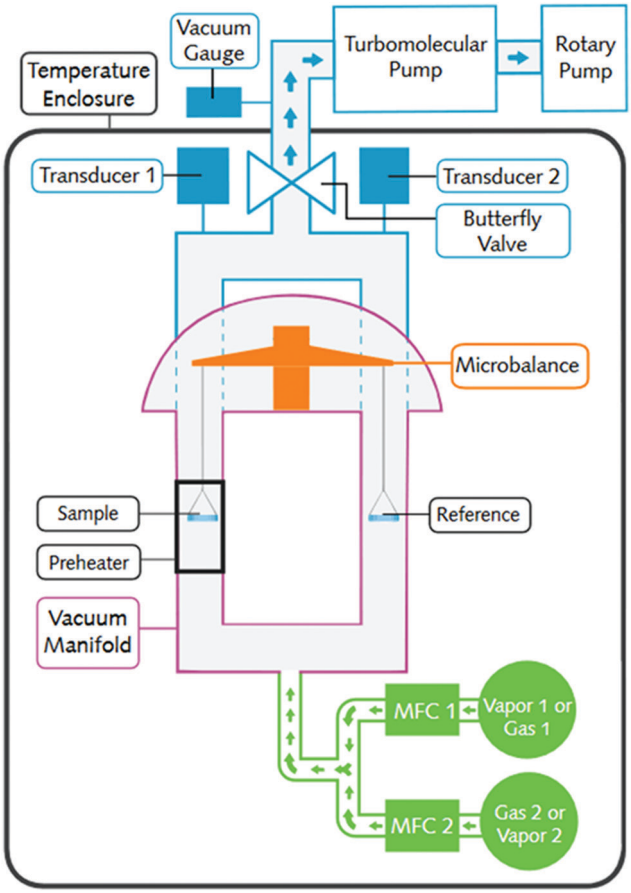

Fig. 4 A simple schematic showing the DVS Vacuum. Used with permission of Surface Measurement Systems.[53]

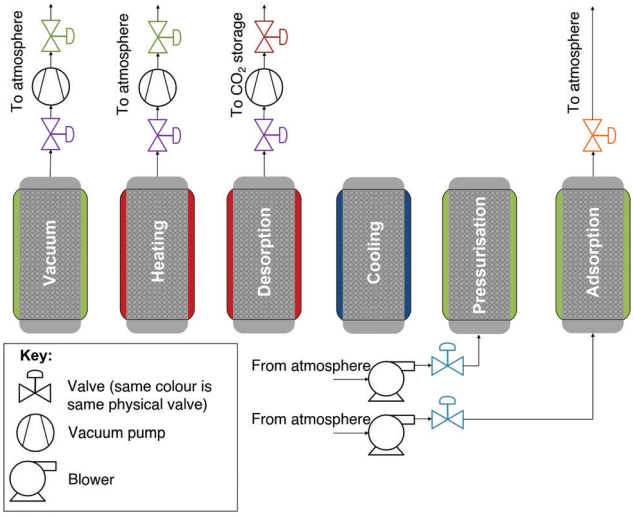

Fig. 5 A schematic of the simple DAC TVSA cycle modelled in the case studies. The valves are highlighted in different colours to represent which valves are the same physical valves.

first equilibrated with H_2O vapour (for both the 30% and 55% RH experiments). Since CO_2 does not affect H_2O adsorption, the H_2O loading and partial pressure will remain constant for the rest of the experiment, given that no more H_2O is added to the chamber. Hence, further pressure increments were implemented using only CO_2, and semi-static mode was used (*i.e.*, no outlet from the chamber). An example dynamic profile of the experiments is shown in the ESI,† Fig. S2.

Tests were also conducted to check whether the assumption applied here would hold up to 80% relative humidity. However, a sharp initial drop in the mass was observed in the dynamic profile of the experiment when CO_2 was added to the chamber, suggesting the desorption of H_2O. We were unable to determine whether the subsequent adsorption was due to CO_2, H_2O, or both. Further experimental work is currently undertaken to study this phenomenon. An example of this profile is shown in Fig. S4. More information about the methodology is available in the ESI.†

4. DAC process modelling

4.1 Process design

Using the calibrated adsorption isotherms, we moved to cycle modelling to understand the impact of co-adsorption descriptions on process performance and to provide an independent benchmark of a TVSA DAC cycle. The cycle modelled is shown in Fig. 5, where the process is a packed-bed TVSA cycle. The steps of the cycle are as follows: vacuum, heating, a second heating step where the product is extracted (desorption), cooling, pressurisation, and adsorption. The cooling step is important to bring the sorbent temperature to below 90 °C before being exposed to air to avoid unnecessary sorbent degradation through oxidation.[52,55,56] This process is similar to the one, without a steam-purge, used by Stampi-Bombelli *et al.* with an extra addition of the short cooling step to prolong the sorbent's lifetime.[13] The process is modelled as a very thin, flat packed bed with length L = 1 cm and diameter D = 10 cm. Although a traditional (column type) packed bed is unlikely to be deployed in a real DAC process, the modelling of a flat packed bed can be a realistic approximation to modelling one of the adsorbent plates described in patents from Climeworks.[57]

4.2 Model assumptions, mass and energy balances

A physical model is required to study the dynamics of adsorption within a packed bed. This will allow the fitting of mass transfer coefficients to experimental data and the study of DAC process performance. The model used in this study closely follows the work by Casas *et al.*[6] Validation work can be found in the ESI,† Fig. S18, where the model results are compared to an earlier temperature swing adsorption study from Joss *et al.*[58]

The key assumptions for the model are as follows:

- The fluid is an ideal gas.
- The flow is described by an axially dispersed plug flow model.
- Radial gradients are neglected.
- There is instantaneous thermal equilibrium between the fluid and solid pellets.

• Mass transfer is described by the linear driving force (LDF) model.[59] The LDF constants are fitted to dynamic data, shown in Fig. S16 and S17 of the ESI.†

• Mass transfer coefficients, axial dispersion coefficients, solid heat capacities, and heats of adsorption are independent of temperature.

• No N_2 is adsorbed,¶ and the non-CO_2/H_2O component of air acts as N_2.

• Pressure drop is described by the Ergun equation.[60]

The overall mass balance is:

$$\frac{\partial}{\partial z}(vc) + \varepsilon_t \frac{\partial c}{\partial t} + (1-\varepsilon_b)\rho_p \sum_i \frac{\partial q_i}{\partial t} = 0 \tag{17}$$

where z [m] is the length along the column, v [m s^{-1}] is the superficial velocity of the fluid, c [mol m^{-3}] is concentration, ε_t [—] is the total void fraction in the column, t [s] is time, ε_b [—] is the void fraction of the bed, ρ_p [kg m^{-3}] is the density of the pellet, and q_i [mol kg^{-1}] is the loading of component i. The component mass balances are:

$$-D_L \varepsilon_b \frac{\partial^2 c_i}{\partial z^2} + \frac{\partial}{\partial z}(vc_i) + \varepsilon_t \frac{\partial c_i}{\partial t} + (1-\varepsilon_b)\rho_p \frac{\partial q_i}{\partial t} = 0 \tag{18}$$

Here D_L [m^2 s^{-1}] is the axial dispersion coefficient, and c_i [mol m^{-3}] is the concentration of component i.

Next, the energy balance is:

$$\begin{aligned} &-\lambda_L \varepsilon_b \frac{\partial^2 T}{\partial z^2} + vcC_{p,f}\frac{\partial T}{\partial z} + \left(\varepsilon_t c C_{p,f} + (1-\varepsilon_b)\rho_p\left(C_{p,s} + C_{p,f}\sum_i q_i\right)\right)\frac{\partial T}{\partial t} \\ &\quad - \varepsilon_t \frac{\partial P}{\partial t} = (1-\varepsilon_b)\rho_p \sum_i \left((-\Delta H_i)\frac{\partial q_i}{\partial t}\right) - \frac{4h_j}{d}(T - T_j) \end{aligned} \tag{19}$$

where λ_L [W m^{-1} K^{-1}] is the axial thermal dispersion coefficient, T [K] is temperature, $C_{p,f}$ [J mol^{-1} K^{-1}] is the molar fluid heat capacity, $C_{p,s}$ [J kg^{-1} K^{-1}] is the mass-based adsorbent heat capacity, P [Pa] is pressure, ΔH_i [J mol^{-1}] is the heat of adsorption for component i, h_j [W m^{-2} K^{-1}] is the global heat transfer coefficient between the jacket and the column, d [m] is the diameter of the column, and T_j [K] is the temperature of the jacket.

A wall energy balance, like the one presented by Casas *et al.*, is not included in this model.[6] Instead, a global heat transfer coefficient is used to predict the heat transfer from the jacket to the inside of the column. We found that this did not significantly affect the model results during validation and substantially improved the computational speed and robustness. However, it does prevent us from calculating the parasitic sensible heat of the contactor. We would like to stress here that the process presented is a hypothetical one to show the effect of co-adsorption, and further detailed design of the contactor would be required to calculate the sensible heat of the contactor accurately.

Other constitutive equations, along with boundary and initial conditions, can be found in the ESI.†

The model calculates the following performance indicators that are relevant to this work:

$$\Phi = \frac{N_{CO_2}}{N_{CO_2} + N_{N_2}} \tag{20}$$

$$\mathrm{Pr} = \frac{N_{CO_2}}{V_{bed}\, t_{cycle}} \tag{21}$$

$$Q_{th} = \frac{\int_{t_{heat,start}}^{t_{des,end}} \frac{\pi {D_b}^2}{4} \int_0^L \frac{4h_L}{D_b}(T_w - T)\mathrm{d}z\mathrm{d}t}{N_{CO_2}} \tag{22}$$

$$W = \frac{\int_{t_{vac,start}}^{t_{vac,end}} \sum_{i=1}^{N_c} n_i(z=L)\frac{1}{\eta_{vac}}\frac{\gamma_{gas}}{1-\gamma_{gas}} RT(z=L)\left(\frac{P_{ambient}}{P(z=L)}^{\frac{\gamma_{gas}-1}{\gamma_{gas}}} - 1\right)\mathrm{d}t}{N_{CO_2}} + \frac{\int_{t_{ads,start}}^{t_{ads,end}} \sum_{i=1}^{N_c} n_i(z=0)\frac{1}{\eta_{blower}}\frac{\gamma_{gas}}{1-\gamma_{gas}} RT(z=0)\left(\frac{P(z=0)}{P_{ambient}}^{\frac{\gamma_{gas}-1}{\gamma_{gas}}} - 1\right)\mathrm{d}t}{N_{CO_2}} \tag{23}$$

where Φ [—] is purity, N_i [mol] is the total number of moles extracted, as a product, of component i in one cycle, Pr [mol m^{-3} s^{-1}] is productivity, V_{bed} [m^3] is the volume of the bed, t_{cycle} [s] is the total cycle time, Q_{th} [J mol^{-1}] is specific heat, $t_{des,end}$ [s] is the time at the end of the desorption step, $t_{heat,start}$ [s] is the time at the start of the heating step, W [J mol^{-1}] is specific work, $t_{vac,end}$ [s] is the time at the end of the vacuum step, $t_{vac,start}$ [s] is the time at the start of the vacuum step, n_i [mol s^{-1}] is the molar flow rate of component i, N_c [—] is the number of components, η_{vac} [—] is the isentropic vacuum pump efficiency, γ_{gas} [—] is the heat capacity ratio of the gas, $t_{ads,end}$ [s] is the time at the end of the adsorption step, $t_{ads,start}$ [s] is the time at the start of the adsorption step, and η_{blower} [—] is the isentropic blower efficiency. Purity is

¶ It is experimentally confirmed that the amount of N_2 adsorbed is very low under ambient conditions (~0.01 mmol g^{-1}). Three isotherms are showing this are found in the ESI,† Fig. S5. Henceforth, we assume no N_2 is adsorbed.

calculated, assuming that all the water can be condensed out in the compression process.

The specific thermal energy is subsequently converted to specific equivalent work *via* the Carnot efficiency as per the guidance of Danaci *et al.*[61] This allows for both forms of specific energy, thermal and work, to be collected into one term. The equation for this conversion is shown in eqn (24).

$$W^{eq} = W + \eta_{turb}\left(1 - \frac{T_L}{T_H}\right)Q_{th} \quad (24)$$

Here W^{eq} [J mol^{-1}] is the specific work equivalent, η_{turb} [—] is an isentropic turbine efficiency, T_L [K] is the lowest temperature that energy can be extracted at, whilst T_H [K] is the temperature of the heating medium in the system. T_L is assumed to equal to the ambient feed temperature, whilst T_H is equal to T_j during the heating step. η_{turb} is taken as 0.75 since Danaci *et al.* state that values between 0.7 and 0.8 are appropriate.[61]

The physical packed-bed column model was implemented in the gPROMS custom modelling suite.[62] The partial differential equations were first discretised using a 2nd order central finite differences method. Next, the index of the equations is reduced according to the Pantelides algorithm to create a solvable set of ordinary differential equations.[63] Finally, these ordinary differential equations were solved using an implicit Runge–Kutta method and a variable time step. Cyclic steady-state conditions are evaluated at 5 equidistant points along the column. Cyclic steady-state is defined as when the loading, composition, pressure and temperature at each of these points at the end of the cycle is within 0.5% of the values at the end of the previous cycle. There is also the option in the model to monitor the percentage of CO_2 saturation reached at the end of the bed during the cycles. This can be used to adjust the adsorption time accordingly, as is done in this work's parametric study.

4.3 Heuristic process optimisation

Finally, a heuristic optimisation was performed in order to compare the performance indicators when using the different co-adsorption isotherm models in the cycle model. The heuristic optimisation approach involves varying many operating variables simultaneously to try and find the optimal design space. To that end, we used gPROMS Global Systems Analysis tool, and more specifically the Monte Carlo-based method function. The baseline case, described fully in Table S9 of the ESI,† is the starting point for this work and is also used to compare the cycle profiles using each co-adsorption isotherm model. Monte Carlo simulations are done varying five main operating variables in the process: vacuum pressure, jacket temperature, heating time, desorption time, and adsorption time. Instead of controlling the adsorption time directly, the percentage of CO_2 saturation reached at the end of the bed is controlled. For each variable, a uniform distribution was assumed between the low and high values. These values are detailed in Table 1.

Table 1 Low and high values for the factors in the heuristic optimisation, where the CO_2 bed saturation parameter is a proxy for adsorption time. This value will be 100% when breakthrough is complete, and investigating higher adsorption times will be pointless. Equally, very low values of this parameter indicate that breakthrough has just begun. Guaranteeing this is above 0% ensures exploring adsorption times that equate to full bed utilisation

Variable	Unit	Low value	High value
P_{vac}	bar	0.1	0.45
$T_{j,heat}/T_{j,des}$	°C	90	100
t_{heat}	s	100	1500
t_{des}	s	18 000	24 000
CO_2 bed saturation ($z = L$, $t = t_{ads,end}$)	%	95	99

Sonnleitner *et al.* found that the stability limit of Lewatit® VP OC 1065 is 90 °C and 110 °C in air and N_2, respectively.[52] It is assumed that oxygen is the reason why the stability limit is much lower in air. By the time the column reaches these temperatures in our baseline case, the column's gas composition is made up of mostly CO_2 and H_2O, so 100 °C is chosen as a maximum limit. This is also the operating limit defined by the manufacturer.[23] The lower limit of vacuum pressure is chosen to be 0.1 bar, as pressures below this value are not typically achieved on an industrial scale. There is no specific limit on the rest of the parameters, and they were chosen after a preliminary investigation into the operating region of interest.

The actual distribution of the factors can be found in the ESI,† which confirms that they are uniform. The one exception to this being the vacuum pressure distribution of the simulations using the Stampi-Bombelli *et al.* model. It was observed that the model struggled to converge at less deep vacuum pressures. However, this is not important as, at these vacuum pressures, the purities using this isotherm model are generally very low, hence the results would not be carried forward for further study. For each isotherm model, 3000 samples are simulated using the cycle model to get a thorough design space coverage.

5. Results and discussion

5.1 Pure component equilibria

The measured experimental isotherms for pure CO_2 and H_2O adsorption are shown in the ESI,† Fig. S6 and S10, respectively, with the desorption branches included. Additionally, the isotherm model fits to the adsorption branches are shown in Fig. S7–S9 and S11 (ESI†), whilst the fitted parameters for CO_2 adsorption are shown in Tables 2 and 3. It was decided that taking hysteresis into account in process modelling would make the cycle model solution unnecessarily complex, and there are questions over how the experimental desorption branches, based only on pressure reduction, would extrapolate to a process where temperature is also being increased.

We shall not go into many details on the pure-component isotherms since they have been explored many times before.[7,8,11,12,15] However, the hysteresis observed for both CO_2 and H_2O isotherms is interesting and for CO_2 adsorption

Table 2 Temperature-dependent Toth model parameters from isotherm fitting. Note that this is for our adjusted version of the Toth model, where the affinity equation no longer includes the reference temperature[a]

Parameter	Value	Unit
T_0	298.15	K
$q_{\infty,0}$	4.86	mol kg^{-1}
χ	0.0000	—
b_0	2.85×10^{-21}	Pa^{-1}
$-\Delta H_0$	117 798	J mol^{-1}
τ_0	0.209	—
α	0.523	—

[a] Limits were imposed on parameters during the fitting process to ensure that the parameters kept their physical meaning. For example, χ is limited to being greater than or equal to 0 to ensure that the maximum capacity did not increase with increasing temperature and so avoided the isotherms crossing.

Table 3 Model parameters fitted to the temperature-dependent GAB model, including correlations in eqn (25) and (26)

Parameter	Value	Unit
q_m	3.63	mol kg^{-1}
C	47 110	J mol^{-1}
D	0.023744	K^{-1}
F	57 706	J mol^{-1}
G	−47.814	J mol^{-1} K^{-1}

measurements this is an unexpected insight. Careful attention was applied to ensuring each point of both the adsorption and desorption branches had reached equilibrium, *e.g.*, by increasing the tolerance to move to a next step (mass change per time) from 0.0015% min^{-1} to 0.0007% min^{-1}. Evidence of this can be seen in the mass change over time gravimetric graph in the ESI,† Fig. S1. Thus, the alternative explanation that equilibrium was not entirely reached before stepping to the next measurement point was tentatively rejected and we believe the hysteresis exhibited is a real phenomenon.

Such hysteresis in CO_2 adsorption on amine-functionalised sorbents has been observed before in a study by Zhou *et al.* in 2014.[64] The adsorbent that the authors studied was an amine functionalised SBA-15. We agree with these authors' suggestion that the hysteresis is potentially due to the strongly chemisorbed species formed on adsorption, and an explanation can be found in the fact that the endothermic direction of the reaction (desorption), has a greater activation energy than the exothermic direction. This also explains how the hysteresis becomes less significant as temperature increases as generally, the energy to overcome this barrier is more likely to exist in the system. Previously, a study by Yu and Chuang has shown that some carbamic acid, the species with the highest heat of adsorption in paired form, is only desorbed using temperature-programmed desorption, supporting the explanation provided here.[27] Meanwhile, the hysteresis loop exhibited in the H_2O isotherms, is common behaviour for multilayer adsorption as a result of metastability of the multilayer in the adsorption branch.[19]

The fitting of the water isotherms was slightly more complicated due to the unknown nature of the relationship between E_1 and E_{2-9} and temperature. A linear relationship was observed between E_{2-9} and temperature in the temperature range studied, much like the latent heat of condensation, E_{10+}. Meanwhile, E_1 appeared to have a concave downwards relationship with temperature meaning the difference between the heat of adsorption of E_1 and E_{2-9} reduces as temperature increases. This is shown in Fig. S12 in the ESI.† Eqn (25) and (26) show the correlations that will fit these two relationships.

$$E_1 = C - \exp(DT) \quad (25)$$

$$E_{2-9} = F + GT \quad (26)$$

where C, D, F, and G are constants. The fitted values of these constants can be found in Table 3.

Additionally, the average isosteric heats of adsorption as calculated from the Clausius–Clapeyron relation using the experimental isotherm data were −70 kJ mol^{-1} and −46 kJ mol^{-1} for CO_2 and H_2O adsorption, respectively.

5.2 Co-adsorption equilibria

Fig. 6 presents the CO_2 isotherm results under wet conditions. Here, we present the uptake enhancement as a function of relative humidity and CO_2 pressure, where the enhancement factor is defined as the CO_2 adsorption under wet conditions divided by the CO_2 adsorption under dry conditions at the same temperature and partial pressure of CO_2. The co-adsorption enhancement effect primarily manifests itself in the lower pressure region with up to 2.5 times the adsorption capacity as under dry conditions. This is of key importance for DAC processes, as they operate adsorption at partial CO_2 pressures of 0.4 mbar. The enhancement seems to asymptote towards unity in the higher-pressure region. Again, this is beneficial for DAC, as desorption commences at significantly higher partial pressures than adsorption (*e.g.*, ∼30 mbar in the baseline case considered in Fig. S12, ESI†).

The observation that the enhancement of CO_2 adsorption occurs mainly at lower CO_2 pressures supports the theory that carbamic acid formation is the main adsorption mechanism on Lewatit® VP OC 1065 as earlier suggested by molecular modelling from Buijs and De Flart.[36] (See Fig. 1b and 2b in Section 2.2.1) If ammonium bicarbonate or hydronium carbamate was formed from ammonium carbamate, the high enhancement factors observed at low partial pressures would be expected to persist at higher partial pressures as each amine group that is used for adsorbing one CO_2 molecule under dry conditions can now adsorb two. (See Fig. 1a and 2a in Section 2.2.1) Indeed, the ϕ_{dry} in the mechanistic model is fitted to have a value of 1, suggesting that under dry conditions the same stoichiometry exists as under wet conditions. In addition, Stampi-Bombelli *et al.* fitted their γ parameter to be 0 on amine-functionalised cellulose, meaning that the maximum adsorption capacity was not affected by water. This is further evidence against an increase in stoichiometry. For these reasons, we believe that paired carbamic acid and water-stabilised carbamic acid are the

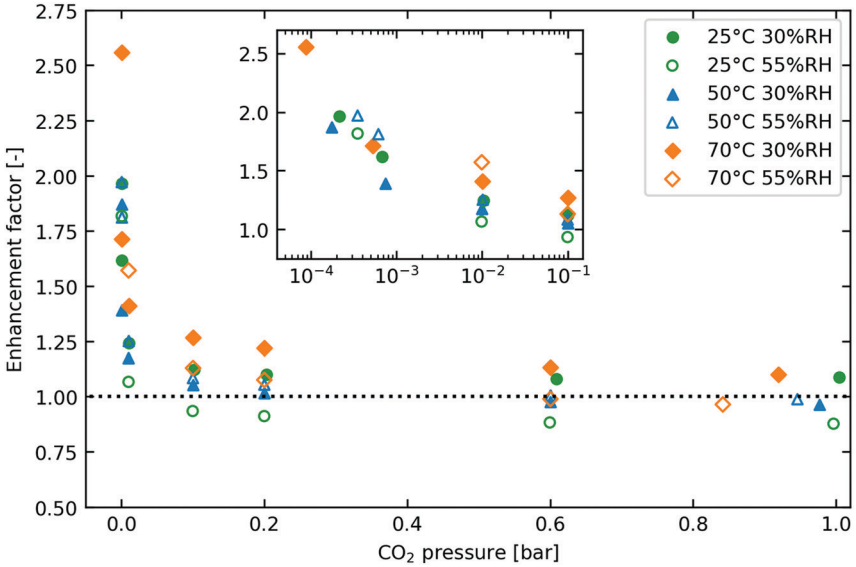

Fig. 6 Enhancement factor of co-adsorption experiments plotted against pressure for a range of temperatures and humidities. Here enhancement factor is defined as amount of CO_2 adsorbed divided by the amount of CO_2 that would be adsorbed under dry conditions at the same temperature and pressure. The isotherm loading values can be found in Fig. 7. Meanwhile, they are converted into amine efficiency in Fig. S13 in the ESI,† using the amine loading of 6.7 mmol g^{-1} reported by Alesi and Kitchin.[37]

two main species formed due to CO_2 adsorption. However, this does not mean that ammonium carbamate cannot form, and this has been proven to happen on other adsorbents.[25,27,29–32] An alternative explanation is that ammonium carbamate forms under dry conditions, but the presence of water promotes carbamic acid formation instead, as suggested by Yu and Chuang.[27]

The co-adsorption results of Fig. 6 also seem to indicate that the higher-humidity experiments sit slightly below the lower-humidity experiments, even reducing the enhancement to below 1 at higher partial pressures, which seems apparent especially for the 25 °C and 70 °C measurements. This would suggest that water can indeed block some amine sites and thereby lower adsorption capacity, as we hypothesised in Section 2.3.1, but it is difficult to say for sure if this is true as this effect was not visible in the 50 °C experiment. The experiments were repeated to check this, with identical results obtained. Therefore, further experimentation including different experimental methods needs to be undertaken: currently, we are running a campaign of breakthrough experiments that could corroborate or reject the findings here.

Fig. 7 and Fig. S14 (ESI†) shows the fit of the experimental data to the two novel co-adsorption models in this work alongside the empirical model from Stampi-Bombelli *et al.*[13] The parameters found in this fitting process are presented in Table 4. It is noted that no model provides a perfect fit, and there is at least one case for each model where a relatively poor fit is found, indicating the known and unknown complexities of co-adsorption and measuring it. When comparing the three models, it is observed that the WADST and the mechanistic model seems to fit the low-pressure region very well. The low-pressure region is most important for DAC, as the partial pressure of CO_2 is always relatively low throughout the cycle, hence this is especially promising. Furthermore, we suggest that there could be changes in the mechanisms at higher CO_2 pressures and this explains why the fitting is generally poorer at the higher-pressure regions. The mechanistic model seems to predict the higher-pressure region better than the WADST model, although the predictions are far from perfect.

Meanwhile, the Stampi-Bombelli *et al.* consistently over-predicts the capacity at the higher two temperatures. We suggest this is due to the model not considering the effect of temperature on the co-adsorption phenomenon. Mathematically, for a given water loading, it is predicting a constant increase in affinity and decrease in capacity at every temperature.

Another important point to make is that the experimental data has sources of potential error. We are trying to elucidate the effect of three parameters (temperature, pressure, and humidity) at once, and there is a possibility for measurement error in all these as well as in the sample mass. Considering this, we should not expect the models to be able to fit the experimental data perfectly.

Finally, when studying the fitted parameters, the value of the critical water loading parameter, A, is very similar in both the WADST model and the mechanistic model. This is noteworthy as it implies that both models predict the same probability of a CO_2 adsorption site having a water molecule available given the same loading of water, which is supportive of our hypotheses on co-adsorption.

5.3 Effect of co-adsorption model selection on process modelling

5.3.1 Effect on working capacity for a fixed cycle. A key question we asked ourselves is if and how the selection of co-

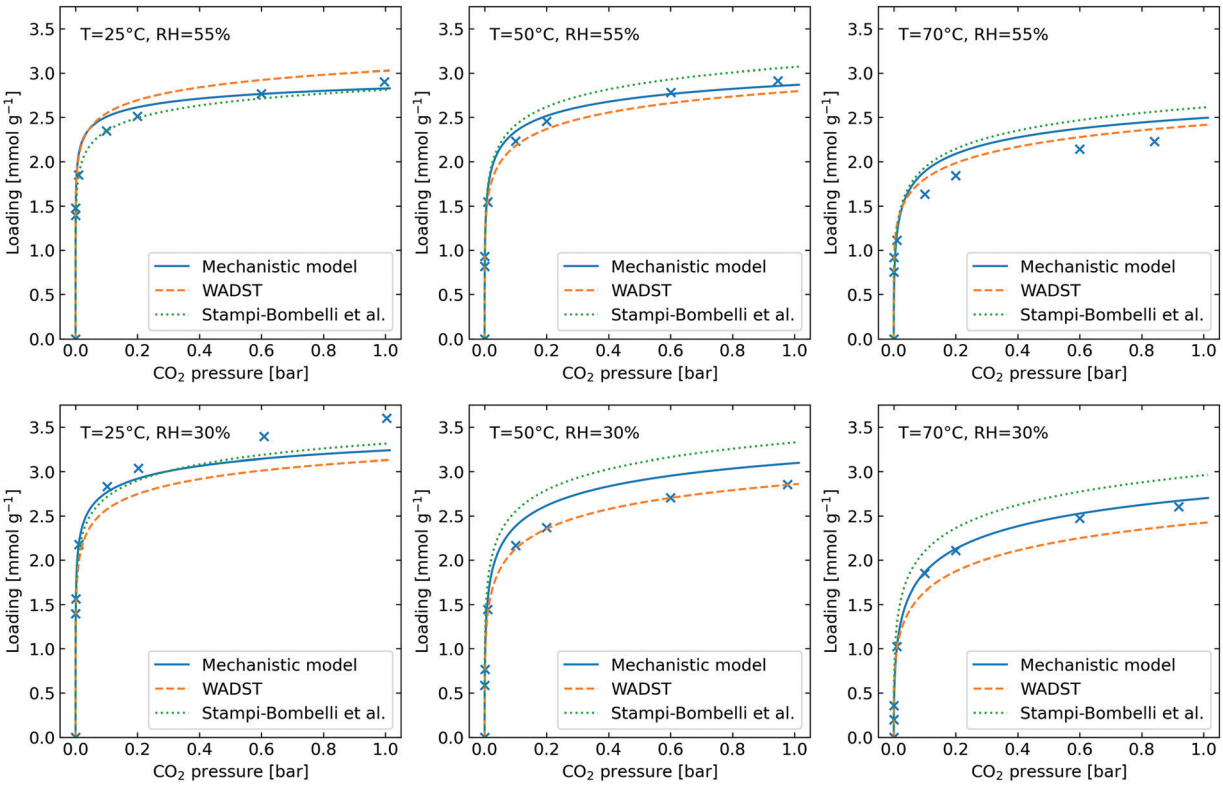

Fig. 7 Experimental co-adsorption CO_2 isotherms (markers), at various temperatures (T) and relative humidities (RH), fitted to an empirical literature co-adsorption model from Stampi-Bombelli *et al.* and the two models presented in this work.[13] The low pressure range of this graph on a log scale is presented in Fig. S14 in the ESI.†

Table 4 Fitted parameters for the empirical literature co-adsorption isotherm model and the two co-adsorption isotherm models presented in this work

Parameter	Value	Unit
Stampi Bombelli *et al.* model		
γ	−0.137	—
β	5.612	—
Mechanistic model		
$f_{\text{blocked.max}}$	0.433	—
k	0.795	kg mol^{-1}
ϕ_{dry}	1.000	—
A	1.535	mol kg^{-1}
$-\Delta H_{\text{wet}}$	130 155	J mol^{-1}
n	1.425	—
WADST model		
$b_{0,\text{wet}}$	1.230×10^{-18}	Pa^{-1}
$q_{\infty,0,\text{wet}}$	9.035	mol kg^{-1}
$\tau_{0,\text{wet}}$	0.053	—
χ_{wet}	0.000	—
α_{wet}	0.053	—
$-\Delta H_{\text{wet}}$	203 687	J mol^{-1}
A	1.532	mol kg^{-1}

adsorption isotherm model influences performance predictions of DAC cycles. Fig. 8 exemplifies how cycle profiles at the column end ($Z = L$) may vary as different co-adsorption isotherm models are used for the baseline DAC cycle specified in the ESI,† Table S9. It is not a surprise that for most of the monitored variables (q_{H_2O}, x, T, and P), there is no significant effect of including a co-adsorption description, the exception being the CO_2 loading and mole fraction. Notably, the loading at the start and the end of the desorption step varies significantly depending on the chosen description. These values influence the working capacity of the material, which is the main difference when considering the cycle profiles. This is important since the working capacity will have a substantial impact on process performance since it is defined as the amount of CO_2 recovered in one cycle. The WADST and mechanistic isotherm models lead to similar predictions of a greater working capacity than when no co-adsorption is included, predicting ∼50% higher loadings during the adsorption step and ∼30% higher loadings after desorption, effectively increasing cyclic working capacity by ∼50%.

In contrast, the Stampi-Bombelli *et al.* approach leads to a similar working capacity to when no co-adsorption is included. This is due to the model assuming that the effect of water loading on the isotherm parameters varies with water loading but not temperature, meaning that this model also predicts higher loadings at desorption conditions. Meanwhile, the WADST and mechanistic models do take the effect of temperature on co-adsorption into account. This leads to the enhancement predicted by the WADST and mechanistic models being higher at the start of the desorption step yet lower at the end than the empirical model predicts.

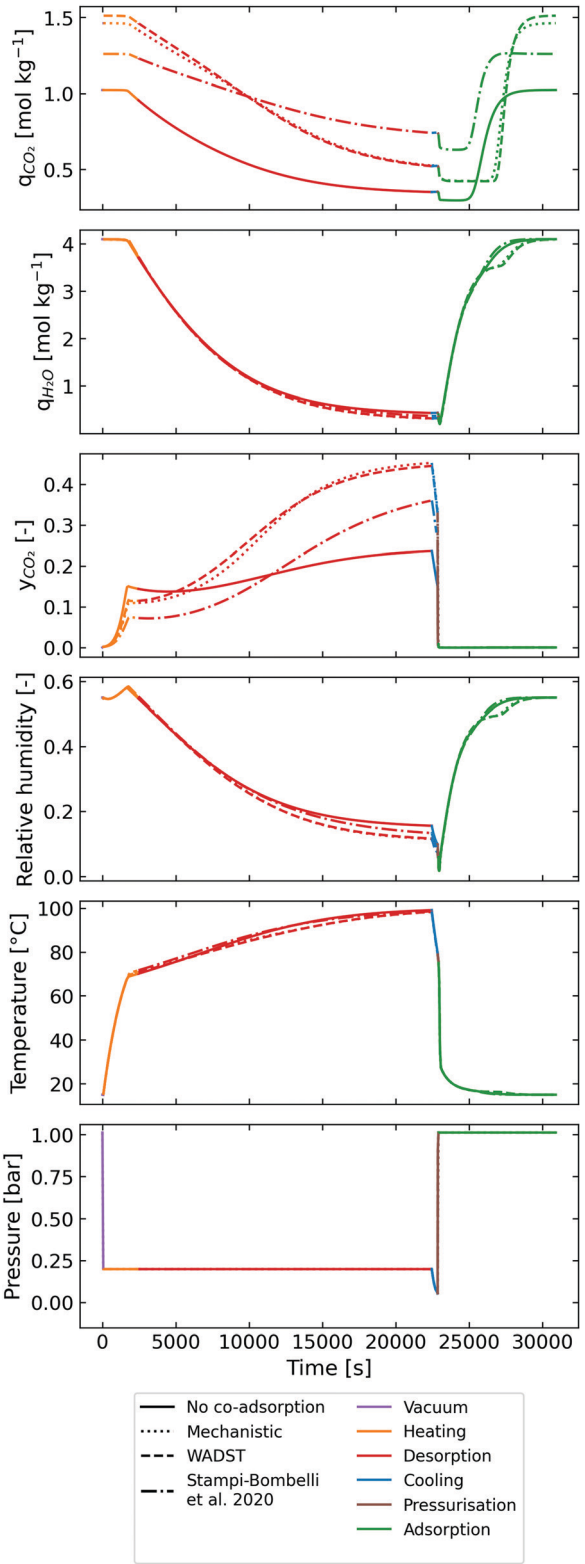

Fig. 8 Modelled cyclic steady-state profiles at the end of an adsorption column ($Z = L$) for the TVSA DAC baseline case using 4 different co-adsorption isotherm models. From top to bottom: CO_2 loading, H_2O loading, CO_2 mole fraction in the gas phase, relative humidity, temperature, and pressure.

5.3.2 Effect on purity, specific work equivalent, and productivity. The effects of co-adsorption and the specific model selection are further exemplified by the heuristic optimisation results, exhibited in Fig. 9. As previously discussed, the working capacity is the primary variable being affected by the co-adsorption description. Hence, the difference in working capacities is a solid explanation of why the distributions vary significantly. However, there are other factors at play. The main one being the shape of the isotherm, which influences the pressure and temperature variation necessary to achieve a specific working capacity.

A good example materialises when comparing the mechanistic and WADST model points, selected as they have identical working capacities, in Table S11 of the ESI.† The mechanistic model predicts that a lower vacuum pressure, longer heating time and longer desorption time are needed to achieve the same working capacities. This is caused by the slight difference in the shape of the isotherm and its dependency on temperature. Essentially, the mechanistic model predicts a higher affinity at higher temperatures. Overall, comparing the mechanistic model to the WADST model (considering the working capacities are identical):

- The lower vacuum pressure leads to a higher electrical energy requirement.
- The overall combined longer heating and desorption time leads to (i) a lower productivity, and (ii) a slightly higher heating requirement, as a slightly higher final temperature is achieved.

This reflects what we see in the distributions with the mechanistic model predicting slightly higher work equivalent and lower productivity. The slight difference in purity is again due to the isotherm shape and can be explained by considering that a longer heating time is required in the mechanistic model case, hence CO_2 starts desorbing at higher temperature. So, the lower purity values predicted are explained by the heating time simply being too short to desorb enough CO_2 to displace the N_2 from the column.

The same arguments can be made when analysing the no co-adsorption, and Stampi-Bombelli *et al.* cases. The Stampi-Bombelli *et al.* model predicts a very steep isotherm at low partial pressures of CO_2 and regeneration temperatures, leading to the requirement for much lower vacuum pressures to achieve comparable working capacities. So, the electrical work, hence work equivalent, is predicted to be much higher than for the other models, and at the same time, the distribution of purity is larger as only the data points with such low vacuum pressures deliver viable purities. The no co-adsorption case predicts the lowest working capacities at optimal conditions leading to distributions of lower productivities and higher specific work equivalent than for the mechanistic and WADST model cases. However, the isotherm is the least steep at low pressures. So, despite the low working capacities, the work equivalent distribution predicted is better than for the Stampi-Bombelli *et al.* case since less extreme vacuum pressures are required to achieve the desired purity. Likewise, this is why the no co-adsorption predicts the largest share of high purities of all the models.

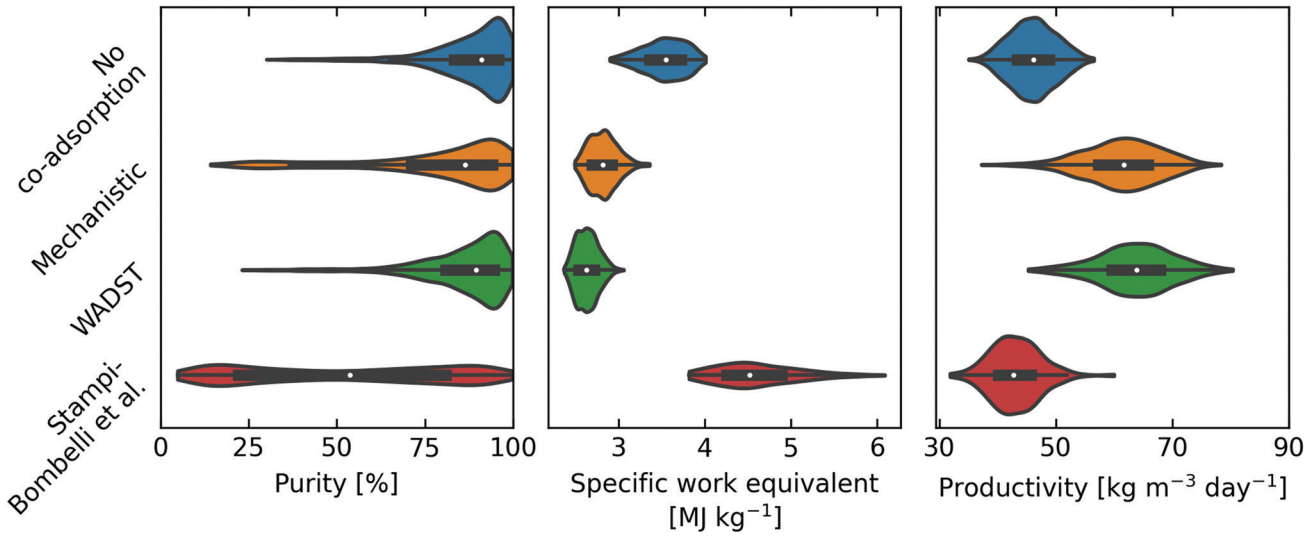

Fig. 9 Violin plots of purity, specific work equivalent, and productivity produced by the parametric study of the TVSA DAC process, using the 4 different approaches to modelling co-adsorption. Specific work equivalent and productivity are shown after removing samples with purity less than 95%. The white dot is the median, the black bar is the interquartile range, the black line is the adjacent values, and the coloured area is the distribution represented by a kernel density estimator.

To summarise, the mechanistic and WADST model predict that co-adsorption improves process performance, in terms of productivity and specific work equivalent, due to the higher achievable working capacities. However, it does make it slightly harder to achieve the required purity, as the isotherms have a larger gradient in the lower-pressure region. Meanwhile, the Stampi-Bombelli *et al.* isotherm model predicts that co-adsorption penalises process performance due to requiring deeper vacuum pressures owing to a higher affinity. It is expected that if a lower vacuum pressure limit was chosen, the Stampi-Bombelli *et al.* model case would achieve the desired purity more easily. This leads to a perhaps obvious but interesting conclusion that there is an optimal gradient in the lower-pressure region. It needs to be steep enough to adsorb CO_2 at such low concentrations, without being too steep, at desorption temperatures and partial pressures, to require very deep vacuum pressures. Meanwhile, this gradient is affected by both the affinity constant, b, of the sorbent in dry conditions, and the humidity.

Overall, the findings of the Stampi-Bombelli *et al.* model are cautiously rejected based on its failure to predict the capacity of the sorbent at higher temperatures, see Section 5.2. However, it does present itself as a valuable option if only the adsorption at one temperature is subject of study.

5.3.3 Optimal cycle designs and operating points. Then, the question of how the co-adsorption models affect optimal cycle design and trends in process performance is answered by investigating Fig. 10 and Fig. S23–S26 in the ESI.† Also in the ESI,† is Table S10, which shows the points from Fig. 10, optimising one of the performance indicators. Fig. 10 shows Pareto fronts of productivity and specific work equivalent predicted using each isotherm modelling approach.

Beginning with the common trends, a higher heating temperature always leads to better performance concerning specific work equivalent and productivity until it reaches the chosen degradation temperature limit of $\sim$100 °C. Furthermore, cycle performance is improved when we run the adsorption step until the sorbent is practically completely saturated, allowing CO_2 to breakthrough at the column end (this is contrary to post-combustion capture, where it is vital to achieve high recoveries, as the main goal is to prevent CO_2 emissions to the atmosphere). Additionally, vacuum pressure and the heating time present a trade-off between productivity and specific work. Operating at a higher vacuum pressure leads to lower specific equivalent work, as a higher proportion of the desorption energy is supplied *via* heat which is less valuable in terms of exergy. However, then a longer heating time – reducing productivity – is needed to ensure that the most of the N_2 is displaced prior to desorption to achieve the desired purity.

Now, considering which co-adsorption models lead to the best DAC performance predictions, the WADST and mechanistic models clearly predict better performance as a result of co-adsorption (for the constraint of greater than 95% purity). The Pareto front is shorter when these co-adsorption descriptions are applied, implying that there is a diminished trade-off between productivity and energy consumption, demonstrating that the operating conditions must be selected more cautiously to find the optimal point. One notable difference as discussed earlier, is the predicted optimal vacuum pressure which is lower when a co-adsorption description is included. It may be worth investigating whether even lower vacuum pressures can be achieved in actual equipment at an industrial scale. The minimum vacuum pressure was chosen as 0.1 bar since it was assumed that it might be significantly harder to achieve lower pressures: in industrial settings, vacuum pressures are usually higher than 0.1 bar.

5.3.4 Benchmark for a solid-sorbent DAC process. Finally, with the previously obtained results and insights, the energy

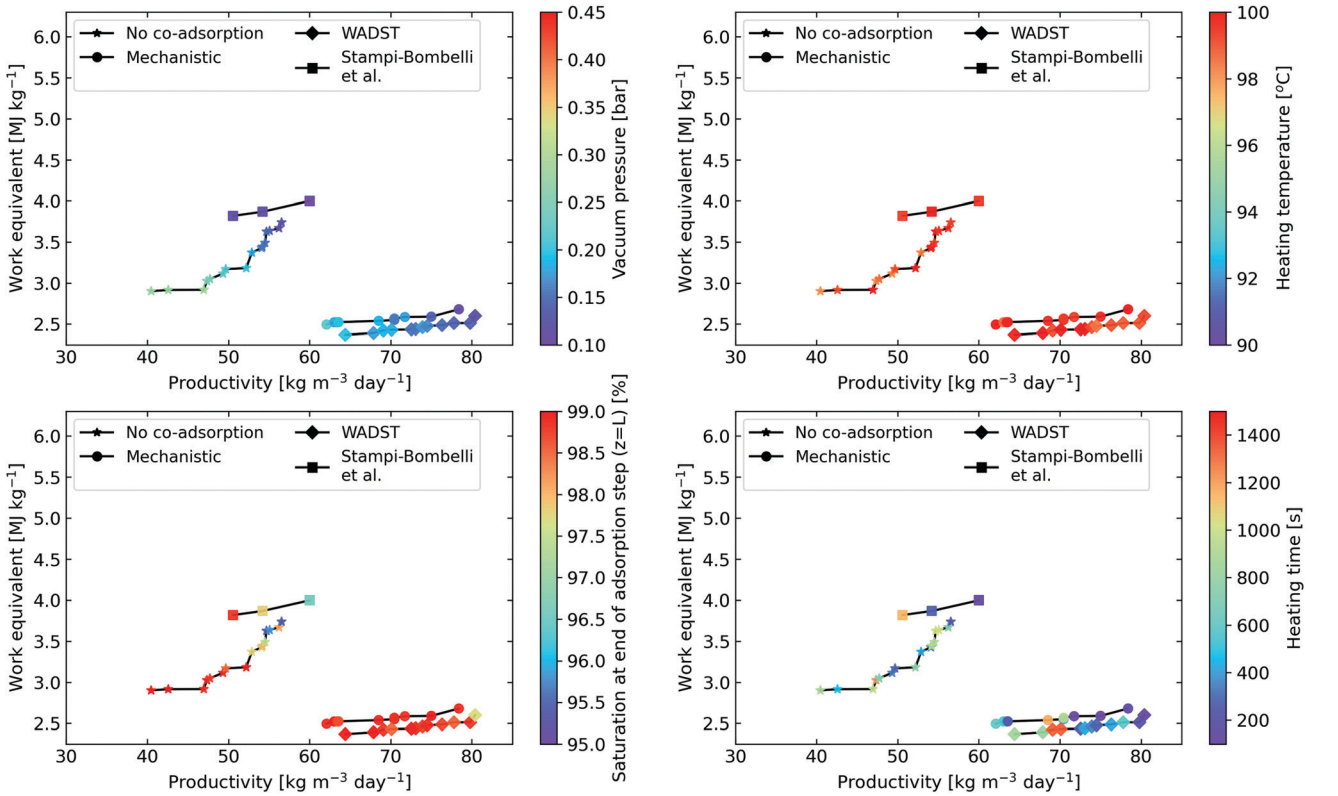

Fig. 10 Pareto fronts of specific work equivalent vs productivity for samples that show a purity of greater than 95% as predicted when applying each co-adsorption isotherm model approach. The operating parameter desorption time is left out, but the trends with desorption time are shown in Fig. S23–S26 in the ESI.† Solid lines added as a guide for the eye. The range of the colour bars is the range investigated in the heuristic optimisation. We see here that the heating temperature converges to the upper bound for all values on the pareto front. A breakdown of the work equivalent contributions for the optimal points can be found in Fig. S27 in the ESI.†

consumption of an optimised DAC process using a commercially available sorbent could be benchmarked.‖ The mechanistic co-adsorption isotherm model is used as its mechanistic nature suggests the highest accuracy when extrapolating beyond measured state parameters. It is also shown to be highly accurate in the all-important lower-pressure regions of the isotherm and is the more conservative out of the two novel co-adsorption isotherm models presented in this work. Here, we shall benchmark the process using specific work equivalent as it represents a useful performance indicator that takes into account the relative values of heat and electricity for a very general case. However, there may be situations, for example, if heat is very cheap due to waste heat being available, when it is more desirable to minimise electrical energy consumption.

Table 5 compares this benchmark case to other DAC technologies in literature. The technologies chosen for comparison are: (i) the Climeworks process using average recorded values recently reported,[65] (ii) two cases of a monolithic adsorption process using novel metal–organic frameworks (MOFs),[66,67] and (iii) a liquid absorption process. The monolithic adsorption case is believed to be a similar technology to that used by Global Thermostat, albeit they are unlikely to be using such a novel adsorbent, meanwhile the liquid absorption case is similar to that used by Carbon Engineering.[69,70]

We believe that using Lewatit® VP OC 1065 in a packed-bed TVSA process represents a realistic benchmark due to the commercial availability of the sorbent and the simple set-up of the process. The calculated heat input into this benchmark is 17% lower than the value reported for Climeworks. This is not unexpected as our case represents a highly ideal and optimised situation. For example, given the Climeworks adsorption bed design (compare, *e.g.*, US patent 2017/0326494 A1),[71] it is not expected that they can fully saturate their bed, as our models predict is the optimal case. Also, their electrical energy consumption is higher by 215%. Explanations for this may lie in the performance of blowers and vacuum equipment having significantly lower efficiencies during real operations, and in bed pressure drop being much higher than predicted by our model (note that our model) assumes a thin layer of sorbent where the air flows through in axial direction, while in the Climeworks contactor, the flow is parallel to the adsorbent sheets, then permeates through the sheet, after which it flows parallel along the sheet to the outlet again. As a result, our

‖ The authors believe that the heuristic optimisation represents a realistic DAC case when a co-adsorption description is included. The only parameter which is still uncertain is the heat transfer coefficient, and experimental data from a scaled-up unit is required to estimate this accurately. In any case, the sensitivity analysis in Fig. S28 of the ESI,† shows that the heat transfer coefficient does not have a large effect on the work equivalent or purity of the process. It does have a significant impact on productivity, however.

Table 5 A comparison of the benchmark, Lewatit® VP OC 1065 minimum work equivalent case, modelled using the mechanistic isotherm model, compared to other DAC technologies. Additionally, the electrical work required to compress CO_2 from atmospheric pressure to 150 bar was calculated in order to compare the adsorption processes to a liquid absorption process that delivers CO_2 at 150 bar. The assumptions for this calculation are found in the ESI

Process	Packed-bed temperature vacuum swing adsorption		Coated monolith temperature vacuum swing adsorption with steam stripping		Liquid absorption
Material	Lewatit® VP OC 1065	Unknown – Climeworks process	MIL-101(Cr)-PEI-800	mmen-Mg_2(dobpdc)	Metal hydroxide
Working capacity [mol kg^{-1}]	0.91	Unknown	0.75	2.55	N/A
Specific heat energy [MJ kg^{-1}]	9.93	11.9	9.68	4.75	5.84
Specific electrical energy [MJ kg^{-1}]	0.80	2.52	0.80	0.73	1.46
Regeneration temperature [°C]	100	~100	100	100	~900
Specific work equivalent [MJ kg^{-1}]	2.49	4.55	2.45	1.54	4.76
Specific work equivalent [MJ kg^{-1}] (with additional compression to 150 bar)	2.93	4.99	2.89	1.98	4.76
Ref.	This work	65	66 and 67	66 and 67	68

benchmark specific work equivalent is lower than for the Climeworks process, suggesting that the Climeworks design could be further optimised to use less electricity and to maximise adsorbent use.

The predicted heat and electrical energy consumption of the monolithic adsorption process utilising MIL-101(Cr)-PEI-800 is similar to that predicted by the benchmark case. However utilising mmen-Mg_2(dobpdc) in a monolithic adsorption process leads to substantially lower heat and electrical energy consumption. The same research group has since shown that mass transfer limitations and the shape of the isotherm could reduce the effectiveness of mmen-Mg_2(dobpdc) for DAC[72] although, if these limitations can be overcome, functionalised MOFs could become effective DAC sorbents.

Last, the liquid absorption process uses less heat than our adsorption benchmark. However, this process is penalised in the work equivalent calculation due to the very high-temperature requirement for regeneration (~900 °C), and as a result, it is the least favourable process using this metric. However it has been noted previously that, currently, the capital costs of this process may be lower than for solid sorbent based DAC.[73]

6. Conclusions

We have developed two novel approaches to modelling the co-adsorption of water and CO_2 onto chemical adsorbents, the 'mechanistic' and 'WADST' models, and showed, using a detailed DAC model, how the choice of (co-)adsorption isotherm significantly influences DAC process performance, as well as presented an independent benchmark of a TVSA process for direct air capture. To this end, we presented a comprehensive set of new pure-component isotherm data for CO_2 and H_2O adsorption on Lewatit® VP OC 1065, as well as co-adsorption isotherm data that shows the enhancement, and potential diminution at higher partial pressures, of CO_2 adsorption in the presence of water. The pure-component experimental data was fitted to the Toth isotherm model for CO_2 adsorption and the GAB isotherm model for water adsorption, the novel mechanistic and WADST co-adsorption models were fitted to the co-adsorption data and a comparison was made with an empirical model presented earlier. The WADST and mechanistic models were especially successful at fitting the co-adsorption data in the crucial lower-pressure region.

It was found that the WADST and mechanistic isotherm models both provide relatively similar results. The DAC cycle performance that they predict is improved due to co-adsorption, where the mechanistic model predicts slightly lower productivity, and higher specific energy input than the WADST model. We presented a benchmark DAC process-sorbent combination using the mechanistic co-adsorption isotherm model, which was chosen due to its (i) accuracy, (ii) mechanistic nature, and (iii) conservative predictions compared to the WADST model. Minimising the energy consumption, the specific work equivalent of the process was found to be 2.49 MJ kg^{-1}, achieving a CO_2 purity of 95.2%. This compares to the Climeworks process's specific work equivalent of 4.55 MJ kg^{-1}, where the difference can likely be explained by the effects of bed saturation, heat losses and inefficiencies that move the real process away from the modelled scenario. Additionally, vital learnings on how to operate solid sorbent based DAC processes were elucidated from the Pareto fronts that resulted from heuristic optimisation. This demonstrated that it is optimal to use a heating temperature as high as this sorbent's stability allowed (100 °C) and run the column until saturation has just been reached. The vacuum pressure, desorption time, and heating time should then be optimised according to the desired purity and desired placement along the Pareto front, *i.e.*, either favouring higher productivity lowering capital costs, or lower energy consumption lowering operating costs.

In conclusion, this study critically showed the importance of including accurate co-adsorption descriptions in process modelling of solid sorbent DAC systems and the considerable effect co-adsorption has on process performance due to varying working capacity and isotherm shape. Further work needs to be done to properly characterise co-adsorption on amine-functionalised sorbents at higher relative humidities, which

are commonly found in the real-world, and study the effect that co-adsorption has on mass transfer, subject of an ongoing investigation. Further to this, a full and independent techno-economic assessment should be performed on this benchmark sorbent-process system to properly benchmark the price of DAC today and to identify opportunities to drive the cost down in the future to support the scale-up of this vital technology.

Author contributions

John Young contributed to the conceptualisation, formal analysis, investigation, methodology, software, validation, visualisation, and writing – original draft. Enrique García-Díez contributed to the investigation, methodology, and writing – review and editing. Susana Garcia contributed to the conceptualisation, formal analysis, funding acquisition, investigation, methodology, and writing – review and editing. Mijndert van der Spek contributed to the conceptualisation, formal analysis, funding acquisition, investigation, methodology, visualisation, and writing – review and editing.

Conflicts of interest

There are no conflicts to declare.

Note added after first publication

This article replaces the version published on 9th August 2021 to include the value of $q_{\infty,0}$ which was missing from Table 2.

Acknowledgements

The research in this article was supported in part by the PrISMa Project (299659), funded through the ACT Programme (Accelerating CCS Technologies, Horizon 2020 Project 294766). Financial contributions from the Department for Business, Energy & Industrial Strategy (BEIS) together with extra funding from the NERC and EPSRC Research Councils, United Kingdom, the Research Council of Norway (RCN), the Swiss Federal Office of Energy (SFOE), and the U.S. Department of Energy are gratefully acknowledged. Additional financial support from TOTAL and Equinor is also gratefully acknowledged.

References

1 V. Masson-Delmotte, P. Zhai, O. Pörtner, D. Roberts, J. Skea, P. R. Shukla, A. Pirani, C. Moufouma-Okia, C. Péan, R. Pidcock, S. Connors, J. B. R. Matthews, Y. Chen, X. Zhou, M. I. Gomis, E. Lonnoy, T. Maycokc, M. Tignor and T. Waterfield, *Global warming of 1.5 °C. An IPCC Special Report on the impacts of global warming of 1.5 °C above pre-industrial levels and related global greenhouse gas emission pathways, in the context of strengthening the global response to the threat of climate change*, 2018.
2 J. C. Minx, W. F. Lamb, M. W. Callaghan, S. Fuss, J. Hilaire, F. Creutzig, T. Amann, T. Beringer, W. de Oliveira Garcia, J. Hartmann, T. Khanna, D. Lenzi, G. Luderer, G. F. Nemet, J. Rogelj, P. Smith, J. L. Vicente Vicente, J. Wilcox and M. del Mar Zamora Dominguez, *Environ. Res. Lett.*, 2018, **13**, 063001.
3 S. Fuss, W. F. Lamb, M. W. Callaghan, J. Hilaire, F. Creutzig, T. Amann, T. Beringer, W. de Oliveira Garcia, J. Hartmann, T. Khanna, G. Luderer, G. F. Nemet, J. Rogelj, P. Smith, J. L. V. Vicente, J. Wilcox, M. del Mar Zamora Dominguez and J. C. Minx, *Environ. Res. Lett.*, 2018, **13**, 063002.
4 M. Fajardy and N. Mac Dowell, *Energy Environ. Sci.*, 2017, **10**, 1389–1426.
5 G. Realmonte, L. Drouet, A. Gambhir, J. Glynn, A. Hawkes, A. C. Köberle and M. Tavoni, *Nat. Commun.*, 2019, **10**, 3277.
6 N. Casas, J. Schell, R. Pini and M. Mazzotti, *Adsorption*, 2012, **18**, 143–161.
7 C. Gebald, J. A. Wurzbacher, A. Borgschulte, T. Zimmermann and A. Steinfeld, *Environ. Sci. Technol.*, 2014, **48**, 2497–2504.
8 R. Veneman, N. Frigka, W. Zhao, Z. Li, S. Kersten and W. Brilman, *Int. J. Greenh. Gas Control*, 2015, **41**, 268–275.
9 N. R. Stuckert and R. T. Yang, *Environ. Sci. Technol.*, 2011, **45**, 10257–10264.
10 Y. Kuwahara, D. Y. Kang, J. R. Copeland, P. Bollini, C. Sievers, T. Kamegawa, H. Yamashita and C. W. Jones, *Chem. – Eur. J.*, 2012, **18**, 16649–16664.
11 R. Serna-Guerrero, Y. Belmabkhout and A. Sayari, *Chem. Eng. J.*, 2010, **161**, 173–181.
12 M. J. Bos, T. Kreuger, S. R. A. Kersten and D. W. F. Brilman, *Chem. Eng. J.*, 2019, **377**, 120374.
13 V. Stampi-Bombelli, M. van der Spek and M. Mazzotti, *Adsorption*, 2020, **26**, 1183–1197.
14 J. Toth, *Acta Chim. Acad. Sci. Hungaricae*, 1971, **69**, 311–317.
15 M. Hefti and M. Mazzotti, *Adsorption*, 2014, **20**, 359–371.
16 M. Hefti and M. Mazzotti, *Ind. Eng. Chem. Res.*, 2018, **57**, 15542–15555.
17 D. Marx, L. Joss, M. Hefti, R. Pini and M. Mazzotti, *Energy Procedia*, 2013, **37**, 107–114.
18 M. Hefti, L. Joss, D. Marx and M. Mazzotti, *Ind. Eng. Chem. Res.*, 2015, **54**, 12165–12176.
19 M. Thommes, K. Kaneko, A. V. Neimark, J. P. Olivier, F. Rodriguez-Reinoso, J. Rouquerol and K. S. W. Sing, *Pure Appl. Chem.*, 2015, **87**, 1051–1069.
20 J. A. Wurzbacher, C. Gebald, S. Brunner and A. Steinfeld, *Chem. Eng. J.*, 2016, **283**, 1329–1338.
21 R. B. Anderson, *J. Am. Chem. Soc.*, 1946, **68**, 686–691.
22 R. B. Anderson and W. Keith Hall, *J. Am. Chem. Soc.*, 1948, **70**, 1727–1734.
23 Lanxess, 2021.
24 P. J. Linstrom and W. G. Mallard, *J. Chem. Eng. Data*, 2001, **46**, 1059–1063.
25 S. A. Didas, M. A. Sakwa-Novak, G. S. Foo, C. Sievers and C. W. Jones, *J. Phys. Chem. Lett.*, 2014, **5**, 4194–4200.
26 Y. Kuwahara, D. Y. Kang, J. R. Copeland, N. A. Brunelli, S. A. Didas, P. Bollini, C. Sievers, T. Kamegawa, H. Yamashita and C. W. Jones, *J. Am. Chem. Soc.*, 2012, **134**, 10757–10760.

27 J. Yu and S. S. C. Chuang, *Energy Fuels*, 2016, **30**, 7579–7587.
28 W. Jung and K. S. Lee, *J. Nat. Gas Sci. Eng.*, 2020, **84**, 103489.
29 U. Tumuluri, M. Isenberg, C. S. Tan and S. S. C. Chuang, *Langmuir*, 2014, **30**, 7405–7413.
30 W. C. Wilfong, C. S. Srikanth and S. S. C. Chuang, *ACS Appl. Mater. Interfaces*, 2014, **6**, 13617–13626.
31 C. S. Srikanth and S. S. C. Chuang, *J. Phys. Chem. C*, 2013, **117**, 9196–9205.
32 X. Wang, V. Schwartz, J. C. Clark, X. Ma, S. H. Overbury, X. Xu and C. Song, *J. Phys. Chem. C*, 2009, **113**, 7260–7268.
33 A. Danon, P. C. Stair and E. Weitz, *J. Phys. Chem. C*, 2011, **115**, 11540–11549.
34 Z. Bacsik, N. Ahlsten, A. Ziadi, G. Zhao, A. E. Garcia-Bennett, B. Martín-Matute and N. Hedin, *Langmuir*, 2011, **27**, 11118–11128.
35 P. Jäger, C. N. Rentzea and H. Kieczka, *Ullmann's Encyclopedia of Industrial Chemistry*, Wiley-VCH Verlag GmbH & Co. KGaA, 2000, pp. 553–560.
36 W. Buijs and S. De Flart, *Ind. Eng. Chem. Res.*, 2017, **56**, 12297–12304.
37 W. R. Alesi and J. R. Kitchin, *Ind. Eng. Chem. Res.*, 2012, **51**, 6907–6915.
38 K. Li, J. D. Kress and D. S. Mebane, *J. Phys. Chem. C*, 2016, **120**, 23683–23691.
39 L. A. Darunte, A. D. Oetomo, K. S. Walton, D. S. Sholl and C. W. Jones, *ACS Sustainable Chem. Eng.*, 2016, **4**, 5761–5768.
40 W. Chaikittisilp, J. D. Lunn, D. F. Shantz and C. W. Jones, *Chem. – Eur. J.*, 2011, **17**, 10556–10561.
41 M. A. Sakwa-Novak and C. W. Jones, *ACS Appl. Mater. Interfaces*, 2014, **6**, 9245–9255.
42 S. A. Didas, A. R. Kulkarni, D. S. Sholl and C. W. Jones, *ChemSusChem*, 2012, **5**, 2058–2064.
43 S. A. Didas, R. Zhu, N. A. Brunelli, D. S. Sholl and C. W. Jones, *J. Phys. Chem. C*, 2014, **118**, 12302–12311.
44 A. Kolmogorov, *Izv. Akad. Nauk USSR Ser. Math.*, 1937, **1**, 355–359.
45 C. W. Price, Acta Metall, *Mater.*, 1990, **38**, 727–738.
46 M. Avrami, *J. Chem. Phys.*, 1939, **7**, 1103–1112.
47 M. Avrami, *J. Chem. Phys.*, 1940, **8**, 212–224.
48 M. Avrami, *J. Chem. Phys.*, 1941, **9**, 177–184.
49 J. Maxwell, *London, Edinburgh, Dublin Philos. Mag. J. Sci. 4th Ser.*, 1860, **19**, 19–32.
50 J. Maxwell, *London, Edinburgh, Dublin Philos. Mag. J. Sci. 4th Ser.*, 1860, **20**, 21–37.
51 J. W. Park, C. U. Kim and W. Isard, *Phys. A*, 2012, **391**, 4883–4890.
52 E. Sonnleitner, G. Schöny and H. Hofbauer, Biomass Convers, *Biorefinery*, 2018, **8**, 379–395.
53 J. P. Young, V. Martis, S. Garcia and M. van der Spek, *11th Trondheim Conf. CO2 Capture, Transp. Storage.*, in press.
54 Surface Measurement Systems, 2021.
55 P. Bollini, S. Choi, J. H. Drese and C. W. Jones, *Energy Fuels*, 2011, **25**, 2416–2425.
56 G. Calleja, R. Sanz, A. Arencibia and E. S. Sanz-Pérez, *Top. Catal.*, 2011, **54**, 135–145.
57 *US 2020/0001224 A9*, 2020.
58 L. Joss, M. Gazzani, M. Hefti, D. Marx and M. Mazzotti, *Ind. Eng. Chem. Res.*, 2015, **54**, 3027–3038.
59 E. Glueckauf, *Trans. Faraday Soc.*, 1955, **51**, 1540–1551.
60 S. Ergun, *Chem. Eng. Prog.*, 1952, **48**, 89–94.
61 D. Danaci, P. A. Webley and C. Petit, *Front. Chem. Eng.*, 2021, **2**, 1–11.
62 Process Systems Enterprise, gPROMS, www.psenterprise.com/products/gproms, 1997-2021.
63 C. C. Pantelides, *SIAM J. Sci. Stat. Comput.*, 1988, **9**, 213–231.
64 L. Zhou, J. Fan, G. Cui, X. Shang, Q. Tang, J. Wang and M. Fan, *Green Chem.*, 2014, **16**, 4009–4016.
65 S. Deutz and A. Bardow, *Nat. Energy*, 2021, **6**, 203–213.
66 A. Sinha, L. A. Darunte, C. W. Jones, M. J. Realff and Y. Kawajiri, *Ind. Eng. Chem. Res.*, 2017, **56**, 750–764.
67 A. Sinha, L. A. Darunte, C. W. Jones, M. J. Realff and Y. Kawajiri, *Ind. Eng. Chem. Res.*, 2020, **59**, 503–505.
68 N. McQueen, M. J. Desmond, R. H. Socolow, P. Psarras and J. Wilcox, *Front. Clim*, 2021, **2**, 38.
69 E. Ping, M. Sakwa-Novak and P. Eisenberger, *Int. Conf. Negat. CO2 Emiss. May 22–24, 2018*, *Göteborg*, *Sweden*, 2018, pp. 1–9.
70 D. W. Keith, G. Holmes, D. Angelo and K. Heidel, *Joule*, 2018, **2**, 1573–1594.
71 *US* 2017/0326494 A1, 2017.
72 L. A. Darunte, T. Sen, C. Bhawanani, K. S. Walton, D. S. Sholl, M. J. Realff and C. W. Jones, *Ind. Eng. Chem. Res.*, 2019, **58**, 366–377.
73 R. Hanna, A. Abdulla, Y. Xu and D. G. Victor, *Nat. Commun.*, 2021, **12**, 368.

